J. Biochem. 2010;148(6):693–703 doi:10.1093/jb/mvq103

JB THE JOURNAL OF BIOCHEMISTRY

Catalysis and oxygen binding of *Ec* DOS: a haem-based oxygen-sensor enzyme from *Escherichia coli*

Received June 22, 2010; accepted August 31, 2010; published online September 21, 2010

Kazuo Kobayashi[1,*], Atsunari Tanaka[2,#], Hiroto Takahashi[2], Jotaro Igarashi[2], Yukako Ishitsuka[2], Nao Yokota[2] and Toru Shimizu[2]

[1]The Institute of Scientific and Industrial Research, Osaka University, Mihogaoka 8-1, Ibaraki, Osaka 567-0047 and [2]Institute of Multidisciplinary Research for Advanced Materials, Tohoku University, 2-1-1 Katahira, Sendai 980-8577, Japan

*Kazuo Kobayashi, The Institute of Scientific and Industrial Research, Osaka University, Mihogaoka 8-1, Ibaraki, Osaka 567-0047, Japan. Tel: +81 6 6879 8501, Fax: +81 6 6876 3287, email: kobayasi@sanken.osaka-u.ac.jp

#Present address: Atsunari Tanaka, The Wistar Institute, Philadelphia, PA19104, USA

A phosphodiesterase (PDE) from *Escherichia coli* (*Ec* DOS) is a novel haem-based oxygen sensor enzyme. Binding of O_2 to the reduced haem in the sensor domain enhances PDE activity exerted by the catalytic domain. Kinetic analysis of oxygen-dependent catalytic enhancement showed a sigmoidal curve with a Hill coefficient value of 2.8. To establish the molecular mechanism underlying allosteric regulation, we analysed binding of the O_2 ligand following reduction of haem in the isolated dimeric sensor domain using pulse radiolysis. Spectral changes accompanying O_2 binding were composed of two phases as a result of reduction of two haem complexes when high-dose electron beams were applied. In contrast, upon reduction of the dimer with a low-dose beam, the kinetics of O_2 ligation displayed single-phase behaviour as a result of the reduction of one haem complex within dimer. Based on these results, we propose that the faster phase corresponds to binding of the first O_2 molecule to one subunit of the dimer, followed by binding of the second O_2 molecule to the other subunit. Notably, for the haem axial ligand mutant proteins, M95A and M95L, O_2 binding displayed single-phase kinetics and was independent of electron beam dose.

Keywords: allosteric control/haem enzyme/oxygen sensor/O_2 binding/pulse radiolysis/phosphodiesterase.

Abbreviations: *Ec* DOS, *Escherichia coli* direct oxygen sensor; *Ec* DOS-PAS, isolated haem-bound PAS domain of *Ec* DOS; PAS, Per (*Drosophila* period clock protein)-Arnt (vertebrate aryl hydrocarbon receptor nuclear translocator)-Sim (*Drosophila* single minded protein); PDE, phosphodiesterase.

Haem-based gas sensors are a class of enzymes that regulate enzymatic activity and DNA binding in response to availability of the diatomic gas molecules, O_2, CO or NO (*1*–*6*). The haem-based gas sensor protein is composed of two functional domains, specifically N-terminal haem-bound sensor and C-terminal catalytic domains. The binding of an external signalling gas molecule to the haem iron complex in the sensor domain leads to changes in the protein structure of that domain. These protein structural changes constitute the second signal, which is transduced to the catalytic domain for regulation of activity of the enzymatic domain. Haem-regulated phosphodiesterase (PDE) from *Escherichia coli* (*Ec* DOS) is a haem-based oxygen sensor enzyme composed of an N-terminal haem-binding sensor domain with a PAS motif and a C-terminal PDE catalytic domain (*6*–*8*). *Ec* DOS displays PDE activity specific for 3′,5′-cyclic diguanylic acid (c-di-GMP) (*9*, *10*), which is significantly enhanced upon binding of O_2 to reduced haem (*11*, *12*). *Ec* DOS is an oxygen sensor enzyme, although catalysis is regulated in response to not only oxygen but also CO and NO concentration. In practice, however, the cellular oxygen concentration should be much higher than the levels of CO or NO (*13*). Structural changes in the haem vicinity caused by oxygen binding to the haem iron are initial events important for gas sensing, followed by intramolecular signal transduction from haem to the catalytic domain and subsequent regulation of PDE activity.

High-resolution X-ray crystallographic structures have been obtained for the Fe^{3+} and oxygen-free Fe^{2+} forms (*14*) as well as the oxygen-bound Fe^{2+} form of isolated haem-bound PAS domains of *Ec*-DOS (*Ec*-DOS-PAS) (Fig. 1) (*15*). The protein folds into a characteristic PAS domain structure and forms a homodimer (*8*). In the Fe^{3+} form, the haem iron interacts with a His 77 side-chain and a hydroxide anion (or water molecule) (Complex I in Fig. 2). Haem iron reduction is accompanied by haem ligand switching from the hydroxide anion (or water molecule) to a side-chain of Met95 from the FG loop (left in Fig. 1, complex IV in Fig. 2). Upon O_2 binding to the Fe^{2+} form, Met95 is replaced by O_2 (right in Fig. 1, complex V in Fig. 2) and the side-chain of Arg97 forms a direct hydrogen bond with the O_2 molecule attached to the Fe^{2+} haem complex. Haem-7-propionate forms a hydrogen bond with Arg97 instead of Met95 in the Fe^{2+}-O_2 complex. The replacement of Met95 with a distal axial ligand perturbs the haem-7-propionate

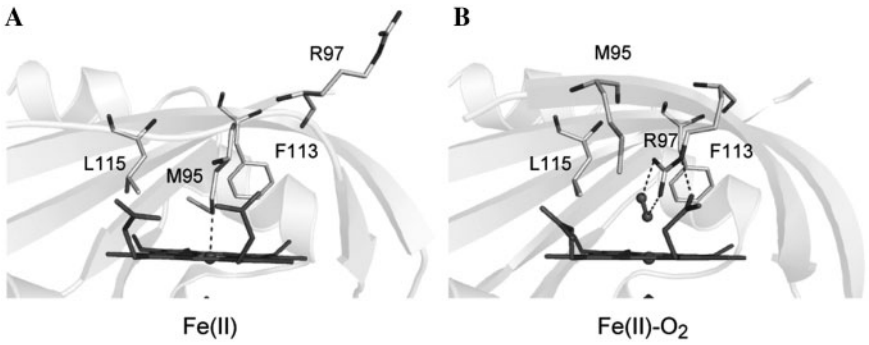

Fig. 1 Crystal structures of the Fe^{2+} A, Protein Data Bank code 1V9Z) and Fe^{2+}-O_2 (B, Protein Data Bank code 1VB6) complexes of *Ec* DOS-PAS.

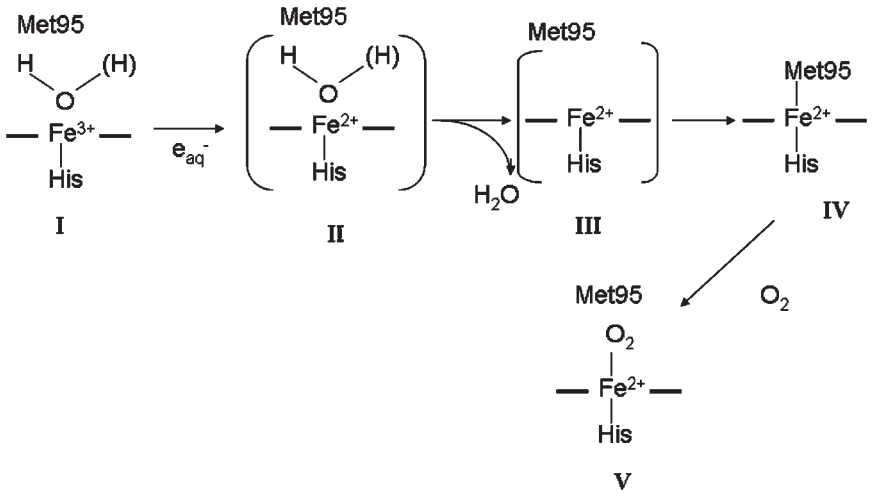

Fig. 2 Structural changes in *Ec* DOS-PAS accompanying iron redox change from the Fe^{3+} to Fe^{2+} haem complex. In complex V, Arg97 forms a hydrogen bond with the oxygen molecule bound to the Fe^{2+} haem complex (cf. Fig. 1) whereas Met95 does not directly interact with the oxygen molecule or the Fe^{2+} haem complex. For pulse radiolysis, the reductant, e, is the aqueous electron, e_{aq}^-.

hydrogen bonding network, resulting in significant conformational changes in the FG loop (*14*). As the enzymatic activities of gas-free M95A and M95L mutant proteins appear similar to that of the gas-activated wild-type enzyme (*12*), it is speculated that global structural changes around Met95 caused by the binding of external ligands or mutations at this position release the catalytic lock and activate catalysis.

Full-length *Ec* DOS is an oligomeric oxygen sensor enzyme. A particular issue of interest is whether enzymatic activity is regulated by O_2-dependent allosteric-ity, similar to that observed for haemoglobin. To elucidate the molecular mechanism of allostericity and the sensing process, that is, the pathway by which perturbation induced by association or dissociation of O_2 is transduced within the haem domain, intermediates generated during this process require characterization. A powerful way to achieve this for haem proteins is the use of time-resolved pulse radiolysis in which a hydrated electron (e_{aq}^-) rapidly reduces the Fe^{3+} haem of various haemoproteins (*16–20*). The pulse radiolysis approach has several features that render it superior over other methods, including the stopped-flow technique. First, pulse radiolysis permits extremely rapid donation of a single electron to a metal centre in an enzyme. The rate of reduction is such that the absence of conformational changes may be assumed (*19*, *20*). Second, pulse radiolysis does not require substrates or chemicals, and thus no complications arise from kinetic constraints imposed by chemical events (*17*). The quaternary structure of methaemoglobin has been characterized by monitoring the kinetics of O_2 binding to the valence hybrid using pulse radiolysis (*21–24*).

In the present study, we demonstrate that the O_2-dependent catalytic activity of *Ec* DOS is allosterically regulated. Pulse radiolysis was applied to reduce haem in *Ec* DOS-PAS, and binding of O_2 was investigated (Fig. 2). The kinetics of O_2 ligation to the haem in the dimer was composed of two phases upon application of a high-dose pulse. However, when one haem group of the dimer was reduced with a low-dose pulse, a single kinetic phase of binding was observed.

Materials and Methods

Materials

All chemical reagents were of the highest available grade. Reagents were purchased from Wako Chemicals (Osaka, Japan), and used without further purification.

Construction of expression plasmids and site-directed mutagenesis

Cloning of *Ec* DOS and construction of the expression plasmid, pET28a(+)-*Ec* DOS-PAS, have been described earlier (*8*, *11*, *12*). All constructs were confirmed by DNA sequencing.

Protein overexpression and purification

Full-length wild-type *Ec* DOS as well as wild-type and mutant *Ec* DOS-PAS proteins were overexpressed in *E. coli* BL21 (DE3) using a pET28a(+) expression plasmid, as described earlier (*12*).

Full-length *Ec* DOS and *Ec* DOS-PAS proteins were purified using column chromatography over nickel-nitrilotriacetic acid-agarose and DEAE, in keeping with a previous report (*12*). All proteins were >95% pure, as assessed using sodium dodecyl sulphate-polyacrylamide gel electrophoresis.

O_2-dependent catalytic activities and spectral changes

Catalytic activities were measured according to a previous report (*12*). O_2-dependent catalytic enhancement was performed under anaerobic conditions in a glove box, except for experiments with 260 μM O_2, which were conducted under air-saturated conditions at 25°C. Formation of the O_2-bound complex during the catalytic measurement was confirmed on the basis of optical absorption spectra (*8*, *12*). Curve fitting was performed with the Hill equation as follows:

$$y = \frac{(K_1 - K_0)}{[1 + (K_2/x)^n] + K_0}$$

where K_0 (minimum in the y axis) = 8.600, K_1 (maximum in the y axis) = 63.89, K_2 (value of the O_2 concentration at half the maximal velocity) = 86.91, n (Hill coefficient) = 2.789.

Pulse radiolysis

Pulse radiolysis experiments were performed using a linear accelerator at the Institute of Scientific and Industrial Research, Osaka University (*19*, *20*, *25–30*). Pulse width and energy were set as 8 ns and 27 MeV, respectively. The light source for the spectrophotometer was a 200 W Xe lamp. After passing through the optical path, transmitted light intensities were analysed and monitored using a fast spectrophotometric system composed of a Nikon monochromator, R-928 photomultiplier (Nikon, Tokyo, Japan), and Unisoku data analysing system (Osaka). For time-resolved transient absorption spectral measurements, the monitored light was focused into a quartz optical fibre, which transported electron pulse-induced transmittance changes to a gated spectrometer (Unisoku, model TSP-601-02) (*30*). The resolution time of the spectrometer was 10 ns.

The concentration of e_{aq}^- generated by pulse radiolysis was determined on absorbance changes at 650 nm using an extinction coefficient of 14.1 mM^{-1} cm^{-1} (*31*). For high-dose experiments, 20–50 μM e_{aq}^- was generated using pulse radiolysis. These concentrations could be adjusted by varying the electron beam dose.

For preparation of pulse radiolysis samples, *Ec* DOS-PAS solutions were treated with 0.1 M *tert*-butyl alcohol (for scavenging OH radicals) in a 10 mM phosphate buffer (pH 7.4), and deoxygenated by repeated evacuation and flushing with argon in a sealed quartz cell. Samples containing O_2 or CO were prepared by mixing argon-saturated buffer solutions with the appropriate volumes of O_2- or CO-saturated buffer solution, respectively. To monitor the reaction of O_2, 50 μl of the O_2-saturated buffer solution was added to the de-aerated 350 μl sample solution containing enzyme and *tert*-butyl alcohol. Quartz cells had an optical path length of 0.3 cm or 1 cm, and the sample temperature was maintained at 25°C. Addition of various concentrations of *tert*-butyl alcohol (0.05–0.2 M) had no effects on O_2 binding or optical absorption spectra of *Ec* DOS-PAS, as reported for other haemoproteins (*16–24*).

O_2 and CO binding were monitored between 0 and 1 s. Ligand binding within this timescale was analysed using the following equation:

$$\Delta A(t) = \alpha e^{-k_1 t} + \beta e^{-k_2 t} \quad (1)$$

where ΔA is the total intensity change at a certain time t, after pulse radiolysis, α and β are initial intensities for each phase, and k_1 and k_2 are the rate constants.

Optical absorption spectra were measured with Hitachi U-3000 (Tokyo, Japan) and Shimadzu UV-1600PC (Kyoto, Japan) spectrophotometers under aerobic and anaerobic conditions, respectively.

Results

Oxygen concentration dependence of the catalytic reaction

To examine how catalytic activity was controlled, the O_2 concentration dependence of catalysis was monitored using the full-length enzyme. As shown in Fig. 3 (filled circles), O_2-dependent catalytic enhancement formed a sigmoidal, thus not hyperbolic, curve. Experimental data were fitted to the calculated Hill plot using a Hill coefficient (n) value of 2.8, suggestive of a regulatory effect for O_2-induced catalytic enhancement. Optical absorption spectra indicated that O_2-binding curve for the full-length enzyme was hyperbolic (vacant triangles and squares in Fig. 3). The half-saturation points for catalysis (EC_{50}) and spectra (K_d) were 87 and 95 μM, respectively.

O_2 binding to wild-type Ec DOS-PAS

Pulse radiolysis experiments involve the instantaneous generation of hydrated electrons (e_{aq}^-), which in turn reduce the haem iron of haemoproteins (*16–19*). The reaction scheme after the reduction of the low-spin Fe^{3+} complex [His-Fe(III)-OH^- or H_2O] of *Ec* DOS-PAS by e_{aq}^- is interpreted to follow the sequence of events illustrated in Fig. 2. A five-coordinate deoxy structure (intermediate III) is formed via the first intermediate (intermediate II) (a six-coordinate ferrous haem with OH^- or H_2O). Subsequently, Met95 in the neighbourhood of the haem coordinates with

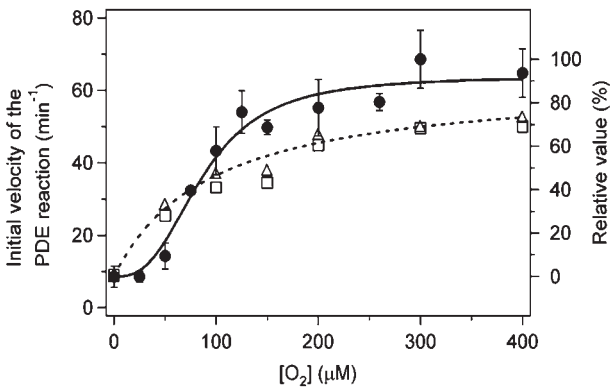

Fig. 3 Regulation of *Ec* DOS catalysis by O_2 binding. O_2 concentration-dependent catalytic enhancement (filled circles) was evaluated, whereas generation of the oxygen-bound form of full-length *Ec* DOS was assessed by optical absorption spectroscopy monitored at 428 nm (vacant triangles, 1 min; vacant squares, 10 min) after mixing with the O_2 buffer. Both experiments were conducted with the protein concentration 0.2 μM in the same Tris–buffer at 25°C. Experiments were repeated at least three times for each data point. Mean values with error bars are presented. Basal catalytic activity in the absence of O_2 was normalized to zero percentage to focus only on the catalytic enhancement that was O_2-induced. The right-hand scale has the percentages of activity used for the evaluation of the Hill plot and of the oxygen-bound forms, whereas the left-hand scale shows actual catalytic activities. Note that the oxygen-bound form did not reach 100% saturation under experimental conditions conducted for catalytic measurements.

ferrous haem as the sixth axial ligand and generates the Fe^{2+} six-coordinated form (IV). The increase in absorbance at 428 nm and decrease at 415 nm reflect this reduction (Fig. 4). Figure 5 illustrates the kinetic difference spectra of the Soret (Fig. 5A) and visible (Fig. 5B) regions after pulse radiolysis of *Ec* DOS-PAS. The spectrum at 10 μs after the pulse is identical to the static difference spectrum of Fe^{2+} minus Fe^{3+} *Ec* DOS-PAS. No appreciable spectral indication of the presence of these intermediates at any wavelength was evident within this timescale. Our findings thus support the formation of the Met95-bound six-coordinated Fe^{2+} haem structure during this time domain.

Spectral changes corresponding to haem reduction in the aerobic solution (with ~130 μM O_2) were monitored. Initial changes in absorption were reversed within a timescale of seconds (Figs 5 and 6A). In particular, the observed decrease in absorption at 560 nm and increase at 580 nm, the characteristic wavelength of Fe^{2+}-O_2 at 1 s (Fig. 5B), account for O_2 binding to Fe^{2+} haem. The time profile was composed of two phases, as shown in Fig. 6A. The rate constants of both the faster and slower phase were dependent on the O_2 concentration (Fig. 6B and C), indicating that the absorbance changes observed in Fig. 6A are a consequence of bimolecular reaction of O_2 with Fe^{2+} *Ec* DOS-PAS. The second-order rate constants of the reaction were calculated as 6.1×10^4 M^{-1} s^{-1} and 3.2×10^3 M^{-1} s^{-1}, respectively. These values are comparable to those obtained using the stopped-flow method (*32*).

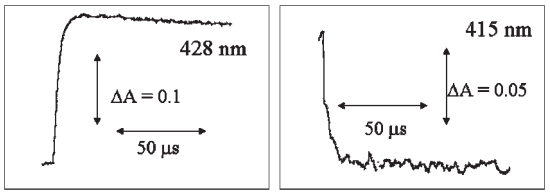

Fig. 4 Absorption changes monitored at 428 nm and 415 nm after pulse radiolysis of *Ec* DOS-PAS. Samples contained 12.5 μM protein and oxygen at a concentration of 130 μM. All samples contained 0.1 M *tert*-butyl alcohol in 10 mM phosphate buffer (pH 7.4). Experiments were performed with a high-dose electron beam (cf. Fig. 6). Experiments were repeated at least three times, and representative data are shown.

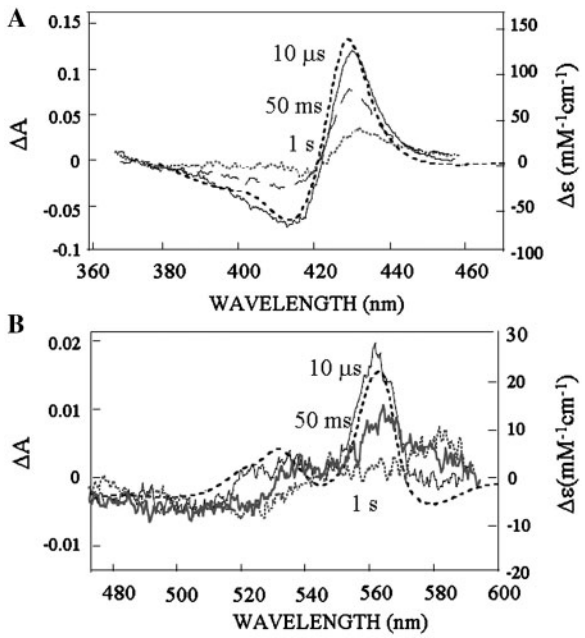

Fig. 5 Kinetic difference (Fe^{3+} minus Fe^{2+}) spectra (broken black lines) for absorption bands between (A) 360 to 460 nm, and (B) 480 to 600 nm at 10 μs, 50 ms and 1 s for wild-type *Ec* DOS-PAS after pulse radiolysis. Samples contained 12.5 μM protein, and 130 μM oxygen. Experiments were performed with a high-dose electron beam (cf. Fig. 3). Note that the left-hand ordinate is in units of ΔA corresponding to kinetic difference spectra, whereas the right-hand ordinate is presented as extinction coefficient units corresponding to [Fe^{2+} minus Fe^{3+}] difference spectra. Experiments were repeated at least three times, and representative data are shown.

The effect of electron beam dose on the rate of oxygen binding to Fe^{2+} haem groups was subsequently investigated. To further evaluate the relationship between the biphasic behaviour and the e_{aq}^- concentration under aerobic conditions, the e_{aq}^- dose was decreased from 25 μM (high dose) to 0.3 μM (low dose) by reducing the electron beam dose at a fixed *Ec* DOS-PAS concentration of 12 μM. The ratios of the fast fraction of total change and fraction of reduced Fe^{2+} in the total haem of the samples were plotted against the e_{aq}^- concentration (Fig. 7C). Using a high-dose electron beam, the time profile was composed of two phases, consistent with previous data (Figs 6 and 7A). The absorbance proportions of the faster and slower phases were approximately equivalent at e_{aq}^- concentrations >12 μM, ~1 equivalent of e_{aq}^- to haem, as highlighted using the vacant circles in Fig. 7C (please note the vertical axis on the right-hand side; only fast-phase fractions are described). Equivalent fractions of both phases were observed at e_{aq}^- concentrations between 10 and 25 μM. The fraction of the fast phase with respect to the total biphasic phase increased with decreasing beam dose (corresponding to the degree of reduced haem) (vacant circles in Fig. 7C). Upon decrease in the e_{aq}^- concentration to below 3 μM, O_2 ligation kinetics displayed single-phase behaviour (Fig. 7B). At low electron beam doses, 15% of haem remained in the Fe^{3+} state (filled circles in Fig. 7C; please see the vertical axis on the left-hand side). Accordingly, it is proposed that under low-dose conditions, a valence-hybrid species designated the 'Fe^{2+}·Fe^{3+} complex' is formed in which only one haem in one dimer subunit is reduced to the Fe^{2+} complex. Note that O_2 binds only to the Fe^{2+} and not the Fe^{3+} complex. Thus, the biphasic character of oxygen binding under high-dose conditions is associated with binding to two different haem species.

We additionally examined the kinetics of CO binding to *Ec* DOS-PAS. Similar results to those obtained when O_2 binding was studied were obtained (please see 'Supplementary data').

O_2 binding to Ec DOS-PAS mutants

Upon O_2 binding to Fe^{2+} haem, Met95 moves away from the haem iron (Figs 1 and 2). Arg97 on the haem-distal side interacts with O_2 bound to Fe^{2+} haem (Fig. 1) (*15*). The X-ray crystal structure of *Ec*

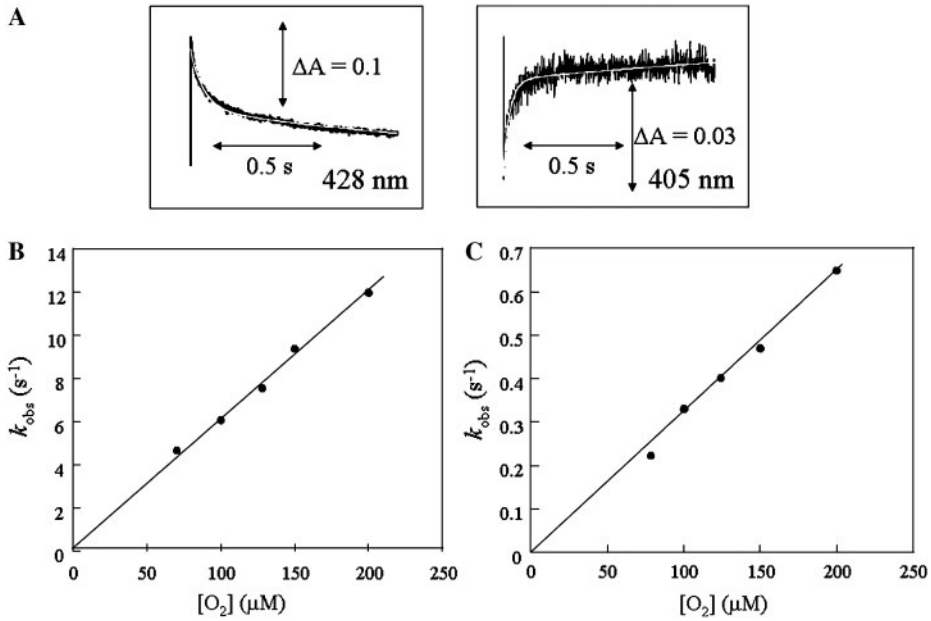

Fig. 6 (A) Absorption spectral changes on a second timescale after pulse radiolysis of *Ec* DOS-PAS monitored at 428 nm (left) and 405 nm (right) at an O_2 concentration of 130 μM. O_2 concentration dependence of rate constants of the faster (B) and slower (C) phases observed after pulse radiolysis. Experiments were performed with a high-dose electron beam. Samples contained 12.5 μM protein and 0.1 M *tert*-butyl alcohol in a 10 mM phosphate buffer (pH 7.4). The white lines represent the curves obtained by double-exponential fitting. Experiments were repeated at least three times, and representative average data are shown. Experimental errors were <20%.

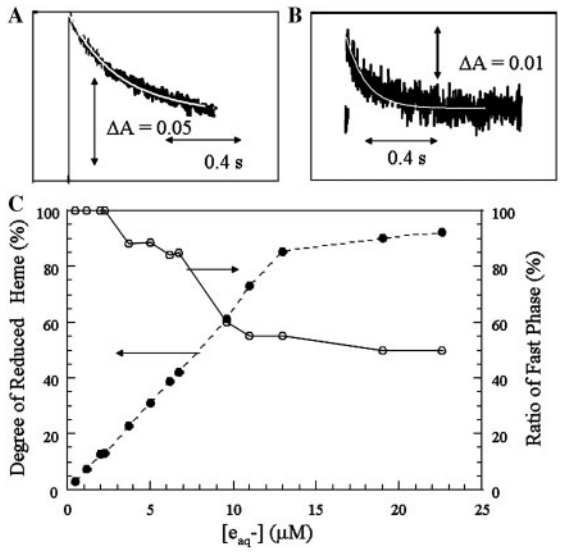

Fig. 7 Dependence on the e_{aq}^- concentration of the fast phase of O_2 binding of wild-type *Ec* DOS-PAS monitored at 428 nm after pulse radiolysis. (A) High dose (22.6 μM e_{aq}^-). The white line is fit to a sum of two exponential functions. (B) Low dose (2.3 μM e_{aq}^-). The white line is fit to one exponential function. Samples contained 12.5 μM enzyme and 130 μM O_2. All samples contained 0.1 M *tert*-butyl alcohol in a 10 mM phosphate buffer (pH 7.4). (C) (-○-) The e_{aq}^- concentration (horizontal axis) dependence of the fast phase fractions of total change accompanied by O_2 binding (vertical axis on the right-hand side) and (—•—) fraction of the reduced (Fe^{2+}) out of the total haem (vertical axis on the left-hand side) in the sample. Experiments were repeated at least three times for each data point. Experimental errors were <20%.

DOS-PAS reveals that Arg97, Phe113 (indirectly) and Leu115 (directly) form a hydrophobic triad in the haem plane or near the ligand access channel of the haem iron (Fig. 1) (*32*, *33*). Mutations altering these residues should influence the O_2-binding process, and it was thus of particular interest to obtain O_2-binding kinetic data on mutant proteins. As with to the wild-type protein, haem in mutant proteins was initially reduced by e_{aq}^- to generate the corresponding Fe^{2+} form (data not shown). Under aerobic conditions, spectral changes accompanying O_2 binding were composed of two phases for the R97A, R97E, R97I, F113T, F113Y, F113L and L115F mutant proteins, and both fast and slow phases were dependent on the O_2 concentration. The rate constants for the fast phase of O_2 binding to these mutant proteins [$3.4 \sim 14 \times 10^4$ M^{-1} s^{-1}] were comparable to that of the wild-type protein [6.1×10^4 M^{-1} s^{-1}]. Similarly, rate constants for the slower phase of O_2 binding to the mutants [$2.0 \sim 17 \times 10^3$ M^{-1} s^{-1}] were close to that of the wild-type protein (3.2×10^3 M^{-1} s^{-1}) (Table I). Additionally, the kinetics of O_2 binding to mutant proteins showed a single phase, with loss of the slower phase, upon application of low-dose electron pulses, similar to that observed with the wild-type protein. Thus, it appears that mutations in Arg97, Phe113 and Leu115 (except for R97I and F113L) have only marginal effects on the kinetics of O_2 binding.

O_2 binding to Met95 mutant proteins is reportedly very rapid, and thus cannot be monitored using the stopped-flow method, except in the case of the M95I protein (*34*), as the reaction is completed within instrumental dead time (*35*). Indeed, mutation of Met95 led to a remarkable increase in the O_2-binding rate, as shown in Fig. 8 and Table I. Notably, unlike the wild-type protein, the M95A, M95I and M95L mutants displayed single-phase O_2 binding at both high and low electron beam doses. At high doses, the

Table I. Rate constants for the binding of oxygen to Fe^{2+} forms of wild-type and mutant *Ec* DOS-PAS proteins measured using pulse radiolysis.

	k_{on} ($\times 10^3$ M^{-1} s^{-1})		
Proteins	**Fast phase**	**Slow phase**	**References**
Wild-type	61	3.2	
	15[a]	–	
	81	8.1	(*32*)
		2.6	(*7*)
M95A	11,000	–	
	5,500[a]		
M95I	5,300	–	
	3,600[a]		
M95L	8,900	–	
	2,700[a]		
M95H	7,500	270	
	820[a]		
R97A	34	2	
	8.2[a]		
R97E	35	2.5	
R97I	140	17	
	100[a]		
F113T	58	6.6	
	20[a]		
F113Y	34	2.1	
	16[a]		
F113L	170	–	
	130[a]		
L115F	68	2.3	
	10[a]		

At least three experiments were performed for each data point, and experimental errors were <20%. [a]The k values were evaluated using a low-dose electron beam; under such conditions, 0.5 mM or lower e_{aq}^- was applied, and only the fast phase fraction was observed (Fig. 6C).

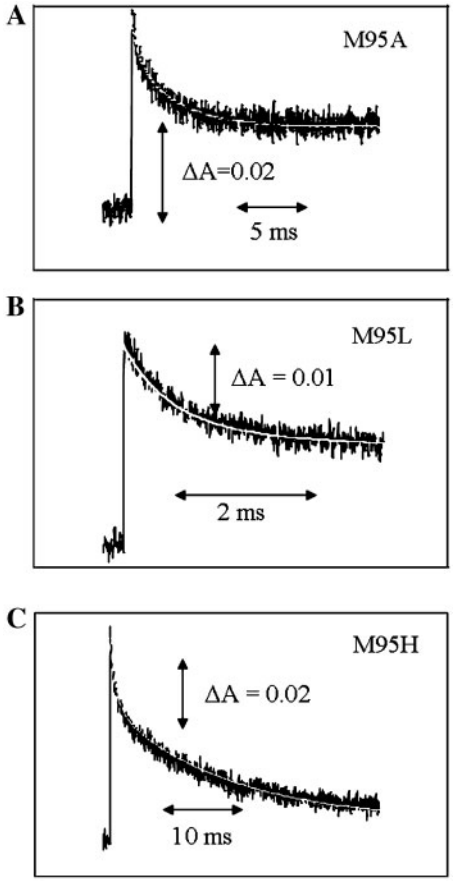

Fig. 8 Absorption spectral changes on a millisecond time domain after pulse radiolysis of M95A (A), M95L (B) and M95H (C) mutant proteins of *Ec* DOS-PAS monitored at 428 nm. The oxygen concentration was 130 μM. Experiments were performed with a high-dose beam (cf. Fig. 6). Samples contained 10.8 μM M95A, 8.7 μM M95L or 12.3 μM M95H. All samples contained 0.1 M *tert*-butyl alcohol in a 10 mM phosphate buffer (pH 7.4). Experiments were repeated at least three times for each spectral change, and representative spectral changes are shown.

O_2-binding rate constants for M95A, M95I and M95L were 1.1×10^7 M^{-1} s^{-1}, 5.3×10^6 M^{-1} s^{-1} and 8.9×10^6 M^{-1} s^{-1}, respectively. Surprisingly, O_2 bound to only one haem in dimeric M95 mutant proteins, even when O_2 was present at high doses. A typical example is shown in Fig. 9, illustrating difference spectra of the M95A mutant at 20 μs, 10 ms and 100 ms after pulse radiolysis. Spectroscopic changes at 10–20 μs reflect reduction of the M95A ferric haem, and the product was identical to that of the ferrous form (black line). The spectrum generated at 10 ms reveals that half the reduced haem (only one haem in the dimer is reduced) can bind O_2. However, no further spectral changes were observed for at least 100 ms, indicating that the other haem of dimeric Fe^{2+} remains O_2-free. For the M95H mutant, the time profile was composed of two phases at high electron beam doses, similar to the wild-type protein (Table I and Fig. 8). The rate constants of both the faster and slower phases for the M95H mutant were dependent on the O_2 concentration (data not shown). The second-order rate constants of the reaction were 7.5×10^6 M^{-1} s^{-1} and 2.7×10^5 M^{-1} s^{-1}, respectively (Table I).

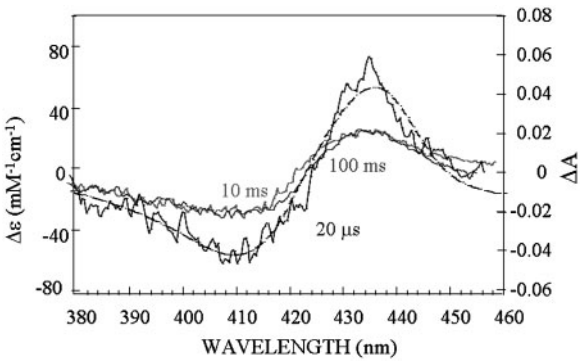

Fig. 9 Kinetic difference (Fe^{3+}minus Fe^{2+}) absorption spectra at 360 to 460 nm at 20 μs, 8 ms and 100 ms, and [Fe^{2+} minus Fe^{3+}] difference spectra (broken black lines) for M95A *Ec* DOS-PAS after pulse radiolysis. The oxygen concentration was 130 μM. Experiments were performed with a high-dose beam (cf. Fig. 6). Note that the right-hand ordinate represents units of ΔA corresponding to kinetic difference spectra whereas the left-hand ordinate represents extinction coefficient units corresponding to [Fe^{2+} minus Fe^{3+}] difference spectra. Experiments were repeated at least three times, and representative data are shown.

Discussion

The O_2-dependent catalytic enhancement experiments, and the spectroscopic O_2 binding work of the present

study (Fig. 3), were performed using the full-length *Ec* DOS enzyme. However, all pulse radiolysis experiments employed *Ec* DOS-PAS, the isolated haem-bound PAS domain of *Ec* DOS. A great deal of biochemical evidence suggests that the full-length *Ec* DOS protein is a tetramer, whereas *Ec* DOS-PAS is a dimer (*6*, *8*, *36*). A recent report suggested, however, that both the full-length *Ec* DOS protein and the *Ec* DOS-PAS protein may be dimers, based on size-exclusion fast protein liquid chromatography coupled with the analysis of multi-angle laser light scattering data (*37*). It is not clear why oligomeric status differs between reports. The His_6-tag was not removed from the protein in the reports cited above, and it may be that the His_6-tag causes variation in the oligomeric status, depending on protein preparation methods and the analytical procedures and methods employed. Also it should be noted that the structure of a haem-sensor protein, wherein haem association/dissociation regulates function in the same manner as gas modulates the activities of gas-sensor proteins, is very flexible, and molecular weight values and/or oligomeric status thus vary with the method of determination (*38*).

The half-saturation point for enhancement of *Ec* DOS activity by O_2 was almost 87 μM, whereas the equilibrium dissociation constant of O_2 for *Ec* DOS was 95 μM (Fig. 3). These values are comparable to the equilibrium dissociation constants (30–140 μM) of O_2 for the other oxygen-sensor enzymes (FixL proteins from *Bradyrhizobium japonicum* and *Rhizobium meliloti*) that contain a similar haem-bound PAS domain (*4*, *35*, *39*, *40*). Such values are much higher than those (0.0029–1.5 μM) of human haemoglobin, sperm whale myoglobin and other haem-bound globin proteins (*35*). Under normal conditions at 1 atmosphere pressure and 25°C, the O_2 concentration in the aqueous solution is almost 260 μM. Even if the O_2 concentration is significantly decreased, to 50 μM, most haemoglobin and myoglobin molecules will still assume the O_2-bound form. However, O_2-sensor proteins with high O_2 dissociation constants of 30–140 μM would efficiently sense the lower O_2 concentration and switch functions on or off. This is why O_2-sensor enzymes show relatively high equilibrium dissociation constants for the O_2 molecule.

The O_2 concentration-dependent catalytic enhancement of *Ec* DOS observed in this study supports the existence of catalytic control (filled circles in Fig. 3). The data of Fig. 3 suggest that significant catalytic enhancement is achieved only after the later binding of the second O_2, rather than after the binding of the first O_2 molecule. The sigmoidal curve may reflect the proportion of molecules, equal to or above a critical value, carrying the second (and later binding) O_2 molecule. It implies that partial O_2 saturation does not trigger a radical change in activity. This behaviour of *Ec* DOS is conceptually similar to that of hemoglobin where the first (and second) O_2 binding significantly enhances affinity of the later O_2 binding.

The hyperbolic (non-co-operative) curve of O_2 binding to full-length *Ec* DOS, obtained by the conventional spectral titration method (Fig. 3), is consistent with that reported by Tuckerman *et al.* (*40*). Additionally, the sigmoidal (co-operative) curve of the O_2-dependent catalytic enhancement of full-length enzyme activity observed in this study (Fig. 3) is also in agreement with the data of Tuckerman *et al.* (*40*). However, Lechauve *et al.* (*37*) observed cooperativity of O_2 binding to the full-length enzyme, using simultaneous measurement of absorption and oxygen tension. The latter method has been used to obtain correct O_2 binding curves for evaluating precise equilibrium O_2 association or dissociation constants to/from oligomeric haemoproteins.

Previous stopped-flow experiments conducted by our group revealed biphasic kinetics of O_2 binding to *Ec* DOS-PAS (*32*). Based on the present data, we propose that the first O_2 molecule binds rapidly to one subunit of the dimer, followed by binding of the second O_2 molecule to the other subunit, leading to a biphasic reaction. CO binding to the enzyme follows similar kinetics. This proposal is supported by the dose dependence of O_2-binding kinetics on electron beam strength, as illustrated in Fig. 10. The sixth haem ligand in Fe^{3+} is OH^- (or a water molecule) (*14*). Upon haem reduction, distal OH^- (or the water molecule) is displaced by Met95 of the FG loop.

Pulse radiolysis permits extremely rapid donation of a single electron to a haem iron in an enzyme. This method facilitates regulation of the electron dose applied to reduce the haem complex and differentiates the haem characteristics of oligomeric haem complexes, as observed for haemoglobin (*20–24*), which renders the technique superior to other chemical and electronic methods involving haem complex reduction. Moreover, high-level electron pulses generated in our facility allows tuning of pulse concentrations over a wide range, from 0.1 μM to 50 μM e_{aq}^-, whereas earlier pulse radiolysis experiments were limited to doses of 1–2 μM e_{aq}^-, making dose-dependence experiments impractical (*21–24*).

At low-dose electron pulses, a ratio of 0.1 for $[e_{aq}^-]$/[*Ec*-DOS-PAS] is too small to permit significant reduction of two haems within dimer, leading to the following equation:

$$Fe^{3+}\cdot Fe^{3+} + e_{aq}^- \rightarrow Fe^{2+}\cdot Fe^{3+}$$

The resulting product is a valence-hybrid species, designated the $Fe^{2+}\cdot Fe^{3+}$ complex, in which only one subunit within each dimer contains reduced Fe^{2+} haem (equation 1 in Fig. 10) (*21–24*). Note that O_2 binds only to the Fe^{2+} complex. Thus, pulse irradiation of a dimer solution in the presence of O_2 (or CO) facilitates the analysis of ligand binding kinetics to a singly reduced subunit within the dimer (equation 2 in Fig. 10). Indeed, the binding kinetics of O_2 (and CO) to the valence hybrid are monophasic. The biphasic character observed with the use of high doses disappeared when the degree of reduction of *Ec* DOS-PAS on a per-haem basis was <15%; this was achieved at low levels (less than 3 μM) of e_{aq}^- (red dots in Fig. 7). Under these conditions, only the fast phase was observed. Therefore, the rate constant

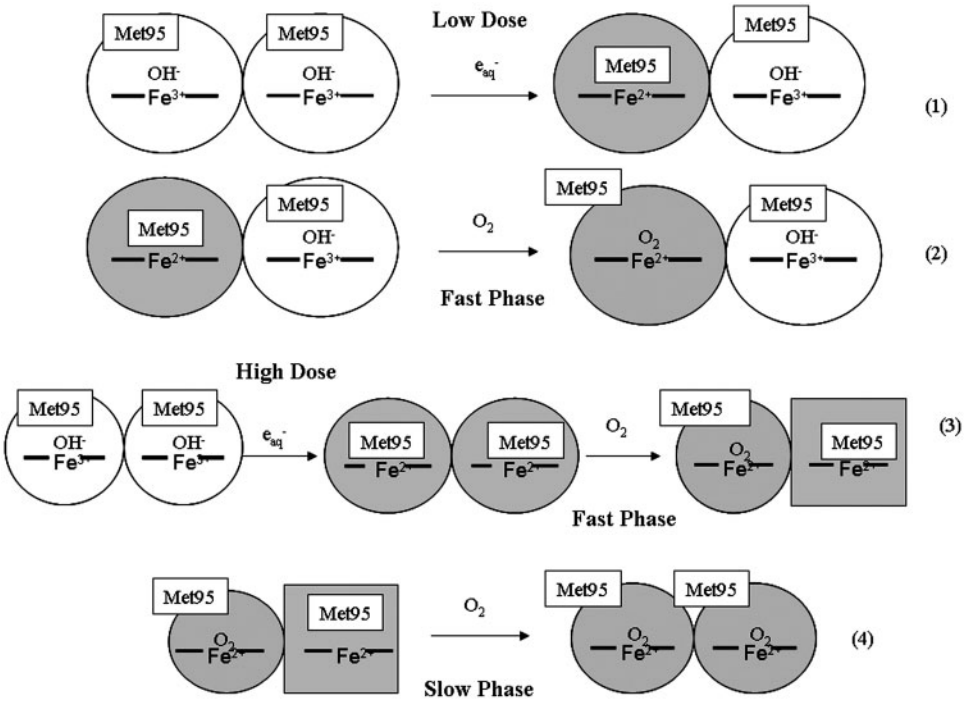

Fig. 10 Redox and coordination structural changes in dimeric *Ec* DOS-PAS after pulse radiolysis. (*1*) and (*2*) depict the proposed redox changes and ligand binding induced by low-dose pulse radiolysis, whereas (*3*) and (*4*) illustrate the proposed redox and ligand binding behaviour using high-dose pulse radiolysis or stopped-flow spectrometry. (*1*) Only one Fe^{3+} haem complex in one subunit of the dimer is reduced by hydrated electrons, e_{aq}^-, leading to the formation of a Fe^{2+}·Fe^{3+} valence hybrid (or heterodimer). (*2*) O_2 binds to the Fe^{2+} complex, generating a Fe^{2+}-O_2·Fe^{3+} heterodimer. Therefore, only a single binding phase is observed. (*3*) After both Fe^{3+} haem complexes are reduced by high-dose hydrated electrons, e_{aq}^-, O_2 initially binds only one of the Fe^{2+} haem complexes, leading to a Fe^{2+}-O_2·Fe^{2+} heterodimer. (*4*) Next, O_2 binds to the Fe^{2+} complex of the Fe^{2+}-O_2·Fe^2 heterodimer, forming a Fe^{2+}-O_2·Fe^{2+}-O_2 homodimer. In high-dose experiments, two binding phases are differentiated, specifically, reaction (*3*) in the fast phase and reaction (*4*) in the slow phase, since the O_2 binding characteristics of each haem complex in the dimer differ and influence each other.

determined under low-dose conditions reflects O_2 binding to the Fe^{2+} complex in the valence hybrid form.

The kinetics of successive O_2 binding to fully reduced dimeric haem can be monitored by both stopped-flow and pulse radiolysis using a high-dose beam (equations 3 and 4 in Fig. 10). Changes in the Met95 coordination structure induced by O_2 binding could result in the movement of the FG loop of *Ec* DOS-PAS, and subsequent transduction of information that affects the ligand-binding affinity state of the other subunit.

Our data imply different O_2 binding characteristics of haem moieties within the two dimer subunits. Specifically, Fe^{2+}·$Fe^{2+}O_2$, in which one O_2 molecule binds to only one subunit of the dimer in the Fe^{2+} state, was isolated, and the X-ray crystal structure determined (*15*). The finding that Fe^{2+}·$Fe^{2+}O_2$ was sufficiently stable to permit crystallization suggests that the K_d value for O_2 binding to the second haem (K^B_d) within the dimer is significantly higher than that for binding to the first haem (K^A_d). The K^B_d value is probably over 300 μM, comparable to that of O_2 binding to the full-length wild-type enzyme (*35*). Whereas Met95 does not bind to the sixth coordination site of either the Fe^{3+} or Fe^{2+}-O_2 form, substantial structural differences should exist between these complexes. O_2 coordination is accompanied by a 7 Å shift in the sulphur atom of Met95, from a haem-coordinated environment to a position where the side-chain points towards the protein surface. Thus, Met95 projects out of the haem pocket in the O_2-bound state (*15*). However, in the Fe^{3+} form, the FG loop is located near the haem-distal side, and this region is highly flexible, as evident from the non-interpretable electron density profile (*14*). Conformational changes caused by axial ligands appear to be less extensive in the Fe^{3+} form. This result is supported by the finding that the activity of the Fe^{3+} form towards c-di-GMP is significantly lower than that of the O_2-bound form (*11*).

A further finding of interest was that O_2 binds to only half of the dimeric M95A and M95L mutant proteins at high pulse doses, unlike what was seen when the wild-type and other mutant enzymes were investigated. In the absence of O_2, the M95A and M95L mutants are five-coordinated high-spin complexes with high catalytic activities, similar to those of gas-bound Fe^{2+} haem enzymes (*12*). Therefore, it appears that significant haem-distal conformational changes do not occur when O_2 binds to one subunit of M95A and M95L mutant proteins.

Stationary and time-resolved resonance Raman spectra indicated that interactions between Met95, Arg97, Phe113 and haem propionates regulate the communication of haem structural changes to the protein moiety involved in the gas-regulated catalytic enhancement of *Ec* DOS (*41*). A flash photolysis study using Arg97 mutant *Ec* DOS proteins confirmed that

such interactions were important for gas-induced structural changes associated with the signal transduction critical for catalytic regulation (*33*). However, in our experiments, mutation of Arg97 or Phe113 had only a marginal effect on conformational changes associated with O_2 binding.

The redox and coordination structural changes induced by pulse radiolysis of *Ec* DOS-PAS are depicted in Fig. 2. However, the hypothetical intermediates, **II** and **III**, could not be detected. The kinetic difference spectrum obtained at 1 μs after the pulse was identical to that of the static reduced enzyme, but not to that of the deoxy form of intermediate **III,** which had an absorption maximum at 435 nm (*32*, *34*, *35*, *42–44*). This indicates that coordination of Met95 with the ferrous haem iron is rapid, being complete within 1 μs. In contrast, after photodissociation of Fe^{2+}-CO via flash photolysis, coordination with Met95 occurred over a 100 μs timescale (*35*, *42–44*). These differences may arise because the side-chain of Met95 is either in, or projects out of, the haem pocket. Met95 may project out of the pocket when CO is bound, as inferred from the X-ray structure of the O_2-bound molecule. However, in the Fe^{3+} form, the FG loop is possibly located near the haem-distal side. In such a situation, the binding of Met95 after reduction of ligand-free Fe^{3+} by pulse radiolysis may occur near, or facing the haem plane. Thus, very rapid rebinding of the flexible Met95 side-chain may take place over a picosecond timescale.

It may appear that an inconsistency exists between the O_2-induced catalytic enhancement (or cooperativity) data (Fig. 3) and the results obtained when O_2 binding to the haem iron complexes was studied (Fig. 10). Rather, we suggest that the dimeric haem complexes are biased (thus asymmetrical) with respect to the redox character (with a low dose of electron beam) and O_2 binding rate (with a high dose of electron beam) (Fig. 10). The allosteric O_2 binding character of *Ec* DOS reported by Lechauve *et al.* (*37*) may help in the understanding of the molecular details of asymmetry in dimeric haem complexes, as seen using pulse radiolysis, and may also explain O_2-induced catalytic cooperativity.

Allosterically controlled O_2 binding is of physiological importance in the catalytic regulation by environmental O_2 in *E. coli* (*39*). Even under *in vivo* aerobic conditions, Fe^{2+}-O_2 is only partially formed. Thus, *Ec*-DOS activity may be critically regulated by the oxygen concentration.

Supplementary data

Supplementary data are available at *JB* Online.

Acknowledgements

We thank the members of the Radiation Laboratory in the Institute of Scientific and Industrial Research, Osaka University, for assistance in operating the linear accelerator.

Funding

The Special Education and Research Expenses (to T.S.) and Grants-in-Aid (to T.S. and K.K.) from the Ministry of Education, Culture, Sports, Science and Technology of Japan.

Conflict of interest

None declared.

References

1. Rodgers, K.R. (1999) Heme-based sensors in biological systems. *Curr. Opin. Chem. Biol.* **3**, 158–167
2. Chan, M.K. (2000) CooA, CAP and allostery. *Nat. Struct. Biol.* **7**, 822–824
3. Aono, S. and Nakajima, H. (1999) Structure and function of CooA, a novel transcriptional regulator containing a *b*-type heme as a CO sensor. *Coord. Chem. Rev.* 190–192, 267–282
4. Gilles-Gonzalez, M.-A. and Gonzalez, G. (2005) Heme-based sensors: defining characteristics, recent developments, and regulatory hypotheses. *J. Inorg. Biochem.* **99**, 1–22
5. Uchida, T. and Kitagawa, T. (2005) Mechanism for transduction of the ligand-binding signal in heme-based gas sensory proteins revealed by resonance Raman spectroscopy. *Acc. Chem. Res.* **38**, 662–670
6. Sasakura, Y., Yoshimura-Suzuki, T., Kurokawa, H., and Shimizu, T. (2006) Structure-function relationships of *Ec*DOS, a heme-regulated phosphodiesterase from *Escherichia coli*. *Acc. Chem. Res.* **39**, 37–43
7. Delgado-Nixon, V.M., Gonzalez, G., and Gilles-Gonzalez, M.A. (2000) Dos, a heme-binding PAS protein from *Escherichia coli*, is a direct oxygen sensor. *Biochemistry* **39**, 2685–2691
8. Sasakura, Y., Hirata, S., Sugiyama, S., Suzuki, S., Taguchi, S., Watanabe, M., Matsui, T., Sagami, I., and Shimizu, T. (2002) Characterization of a direct oxygen sensor heme protein from *E. coli*: effects of the heme redox states and mutations at the heme binding site on catalysis and structure. *J. Biol. Chem.* **277**, 23821–23827
9. Méndez-Oritz, M.M., Hyodo, M., Hayakawa, Y., and Membrillo-Hernández, J. (2006) Genome-wide transcriptional profile of *Escherichia coli* in response to high levels of the second messenger 3′, 5-cyclic diguanylic acid. *J. Biol. Chem.* **281**, 8090–8099
10. Schmidt, A.J., Ryjenkov, D.A., and Gomelsky, M. (2005) The ubiquitous protein domain EAL is a cyclic diguanylate-specific phosphodiesterase: enzymatically active and inactive EAL domains. *J. Bacteriol.* **187**, 4774–4781
11. Takahashi, H. and Shimizu, T. (2006) Phosphodiesterase activity of *Ec* DOS, a heme-regulated enzyme from *Escherichia coli*, toward 3′,5′-cyclic diguanylic acid is obviously enhanced by O_2 and CO binding. *Chem. Lett.* **35**, 970–971
12. Tanaka, A., Takahashi, H., and Shimizu, T. (2007) Critical role of the heme axial ligand, Met95, in locking catalysis of the phosphodiesterase from *Escherichia coli* (*Ec* DOS) toward cyclic diGMP. *J. Biol. Chem.* **282**, 21301–21307
13. Huang, S.H., Rio, D.C., and Marletta, M.A. (2007) Ligand binding and inhibition of an oxygen-sensitive soluble guanylate cyclase, Gyc-88E, from *Drosophila*. *Biochemistry* **46**, 15115–15122
14. Kurokawa, H., Lee, D.S., Watanabe, M., Sagami, I., Mikami, B., Raman, C.S., and Shimizu, T. (2005) A redox-controlled molecular switch revealed by the crystal

structure of a bacterial heme PAS sensor. *J. Biol. Chem.* **279**, 20186–20193
15. Park, H.J., Suquet, C., Satterlee, J.D., and Kang, C. (2004) Insights into signal transduction involving PAS domain oxygen-sensing heme proteins from the X-ray crystal structure of *Escherichia coli* Dos heme domain (*Ec* DosH). *Biochemistry* **43**, 2738–2746
16. Land, E.J. and Swallow, A.J. (1971) One-electron reactions in biochemical systems as studied by pulse radiolysis: V. Cytochrome. *c. Arch. Biochem. Biophys.* **145**, 365–372
17. Kobayashi, K. and Hayashi, K. (1981) One-electron reduction in oxyform of hemoproteins. *J. Biol. Chem.* **256**, 12350–12354
18. Kobayashi, K., Amano, M., Kanbara, Y., and Hayashi, K. (1987) One-electron reduction of the oxyform of 2,4--diacetyldeuterocytochrome P-450$_{cam}$. *J. Biol. Chem.* **262**, 5445–5447
19. Nakajima, H., Nakagawa, E., Kobayashi, K., Tagawa, S., and Aono, S. (2001) Ligand-switching intermediates for the CO-sensing transcriptional activator CooA measured by pulse radiolysis. *J. Biol. Chem.* **276**, 37895–37899
20. Kobayashi, K., Koppenhöfer, A., Ferguson, S.J., and Tagawa, S. (1997) Pulse radiolysis studies on cytochrome cd_1 nitrite reductase from Thiosphaera pantotropha: evidence for a fast intramolecular electron transfer from *c*-heme to d_1-heme. *Biochemistry* **36**, 13611–13616
21. Rollema, H.S., Scholberg, H.P.F., de Bruin, S.H., and Raap, I.A. (1976) The kinetics of carbon monoxide binding to partially reduced methemoglobin. *Biochem. Biophys. Res. Commun.* **71**, 997–1003
22. Ilan, Y.A., Samuni, A., Chevion, M., and Czapski, G. (1978) Quaternary states of methemoglobin and its valence-hybrid: a pulse radiolysis study. *J. Biol. Chem.* **253**, 82–86
23. Chevion, M., Ilan, Y.A., Samuni, A., Navok, T., and Czapski, G. (1979) Quaternary structure of methemoglobin: pulse radiolysis study of the binding of oxygen to the valence hybrid. *J. Biol. Chem.* **254**, 6370–6374
24. Raap, A., van Leeuwen, J.W., van Eck-Schouten, T., Rollema, H.S., and de Bruin, S.H. (1977) Heterogeneity in the kinetics of oxygen binding to partially reduced human methemoglobin. *Eur. J. Biochem.* **81**, 619–626
25. Kobayashi, K. and Hayashi, K. (1990) Reduction of the oxy form in hemoproteins to the ferryl form. *J. Am. Chem. Soc.* **112**, 6051–6053
26. Suzuki, S., Kohzuma, T., Deligeer, Yamaguchi, K., Nakamura, N., Shidara, S., Kobayashi, K., and Tagawa, S. (1994) Pulse radiolysis studies on nitrite reductase from *Achromobacter cycloclastes* IAM 1013: evidence for intramolecular electron transfer from Type 1 Cu to Type 2 Cu. *J. Am. Chem. Soc.* **116**, 11145–11146
27. Kobayashi, K., Tagawa, S., Daff, S., Sagami, I., and Shimizu, T. (2001) Rapid calmodulin-dependent interdomain electron transfer in neuronal nitric-oxide synthase measured by pulse radiolysis. *J. Biol. Chem.* **276**, 39864–39871
28. Kobayashi, K. and Tagawa, S. (2003) Direct observation of guanine radical cation deprotonation in duplex DNA using pulse radiolysis. *J. Am. Chem. Soc.* **125**, 10213–10218
29. Kobayashi, K., Mostafa, G., Tagawa, S., and Yamada, M. (2005) Transient formation of a neutral ubisemiquinone radical and subsequent intramolecular electron transfer to pyrroloquinoline quinone in the *Escherichia coli* membrane-integrated glucose dehydrogenase. *Biochemistry* **44**, 13567–13572
30. Mustafa, G., Ishikawa, Y., Kobayashi, K., Migita, C.T., Elias, M.D., Nakamura, S., Tagawa, S., and Yamada, M. (2008) Amino acid residues interacting with both the bound quinone and coenzyme, pyrroloquinoline quinone, in *Escherichia coli* membrane-bound glucose dehydrogenas. *J. Biol. Chem.* **283**, 22215–22221
31. Gordon, S. and Hart, E.J. (1964) Spectrophotometric detection of hydrated electrons in Co^{60} γ-ray irradiated solutions. *J. Am. Chem. Soc.* **86**, 5343–5344
32. Yokota, N., Araki, Y., Kurokawa, H., Ito, O., Igarashi, J., and Shimizu, T. (2006) Critical roles of Leu99 and Leu115 at the heme distal side in auto-oxidation and the redox potential of a heme-regulated phosphodiesterase from *Escherichia coli*. *FEBS J.* **273**, 1210–1223
33. Ishitsuka, Y., Araki, Y., Tanaka, A., Igarashi, J., Ito, O., and Shimizu, T. (2008) Arg97 at the heme distal side of the isolated heme-bound PAS domain of a heme-based oxygen sensor from *Escherichia coli* (*Ec* DOS) plays critical roles in auto-oxidation and binding to gases, particularly O_2. *Biochemistry* **47**, 8874–8884
34. Gonzalez, G., Dioum, E.M., Bertolucci, C.M., Tomita, T., Ikeda-Saito, M., Cheesman, M.R., Watmough, N.J., and Gilles-Gonzalez, M.-A. (2002) Nature of the displaceable heme-axial residue in the *Ec*Dos protein, a heme-based sensor from *Escherichia coli*. *Biochemistry* **41**, 8414–8421
35. Taguchi, S., Matsui, T., Igarashi, J., Sasakura, Y., Araki, Y., Ito, O., Sugiyama, S., Sagami, I., and Shimizu, T. (2004) Binding of oxygen and carbon monoxide to a heme-regulated phosphodiesterase from *Escherichia coli*: kinetics and infrared spectra of the full-length wild-type enzyme, isolated PAS domain and Met95 mutants. *J. Biol. Chem.* **279**, 3340–3347
36. Yoshimura, T., Sagami, I., Sasakura, I., and Shimizu, T. (2003) Relationships between heme incorporation, tetramer formation, and catalysis of a heme-regulated phosphodiesterase from *Escherichia coli*: a study of deletion and site-directed mutants. *J. Biol. Chem.* **278**, 53105–53111
37. Lechauve, C., Bouzhir-Sima, L., Yamashita, T., Marden, M.C., Vos, M.H., Liebl, U., and Kiger, L. (2009) Heme ligand binding properties and intradimer interactions in the full-length sensor protein DOS from *Escherichia coli* and its isolated heme domain. *J. Biol. Chem.* **284**, 36146–36159
38. Miksanova, M., Igarashi, J., Minami, M., Sagami, I., Yamauchi, S., Kurokawa, H., and Shimizu, T. (2006) Characterization of heme-regulated eIF2α kinase: roles of the N-terminal domain in the oligomeric state, heme binding, catalysis and inhibition. *Biochemistry* **45**, 9894–9905
39. Gilles-Gonzalez, M.A. and Gonzalez, G. (2004) Signal transduction by heme-containing PAS-domain proteins. *J. Appl. Phys.* **96**, 774–783
40. Tuckerman, J.R., Gonzalez, G., Sousa, E.H.S., Wan, X., Saito, J.A., Alam, M., and Gillez-Gonzalez, M.A. (2009) An oxygen-sensing diguanylate cyclase and phosphodiesterase couple for c-di-GMP control. *Biochemistry* **48**, 9764–9774
41. El-Mashtoly, S.F., Nakashima, S., Tanaka, A., Shimizu, T., and Kitagawa, T. (2008) Roles of Arg97 and Phe113 in regulation of distal ligand binding to heme in the sensor domain of *Ec* DOS protein: resonance

Raman and mutation study. *J. Biol. Chem.* **283**, 19000–19010
42. Liebl, U., Bouzhir-Shima, L., Négrerie, M., Martin, J.-L., and Vos, M.H. (2002) Ultrafast ligand rebinding in the heme domain of the oxygen sensors FixL and Dos: general regulatory implications for heme-based sensors. *Proc. Natl Acad. Sci. USA* **99**, 12771–12776
43. Liebl, U., Bouzhir-Shima, L., Kinger, L., Marden, M.C., Lambry, J.-C., Négrerie, M., and Vos, M.H. (2003) Ligand binding dynamics to the heme domain of the oxygen sensor Dos from *Escherichia coli*. *Biochemistry* **42**, 6527–6535
44. Yamashita, T., Bouzhir-Shima, L., Lambry, J-C., Liebl, U., and Vos, M.H. (2008) Ligand dynamics and early signaling events in the heme domain of the sensor protein Dos from *Escherichia coli*. *J. Biol. Chem.* **283**, 2344–2352